Chapter 27

Spectrally Resolved FRET Microscopy of α-Synuclein Phase-Separated Liquid Droplets

Jaladhar Mahato, Soumik Ray, Samir K. Maji, and Arindam Chowdhury

Abstract

Liquid-liquid phase separation (LLPS) has emerged as an important phenomenon associated with formation of membraneless organelles. Recently, LLPS has been shown to act as nucleation centers for disease-associated protein aggregation and amyloid fibril formation. Phase-separated α-synuclein droplets gradually rigidify during the course of protein aggregation, and it is very challenging to understand the biomolecular interactions that lead to liquid-like to solid-like transition using conventional ensemble measurements. Here, we describe a spectrally-resolved fluorescence microscopy based Förster resonance energy transfer (FRET) imaging to probe interactions of α-synuclein in individual droplets during LLPS-mediated aggregation. By acquiring entire emission spectral profiles of individual droplets upon sequential excitation of acceptors and donors therein, this technique allows for the quantification of sensitized emission proportional to the extent of FRET, which enables interrogation of the evolution of local interactions of donor-/acceptor-labeled α-synuclein molecules within each droplet. The present study on single droplets is not only an important development for studying LLPS but can also be used to investigate self-assembly or aggregation in biomolecular systems and soft materials.

Key words Liquid-liquid phase separation, α-synuclein, Domain interaction, Biomolecular interactions, Liquid droplet aging, Sensitization imaging, Spectrally-resolved FRET microscopy

1 Introduction

A living cell makes membraneless compartments to organize and sequester biomolecules (proteins and nucleic acids) for a wide range of functionalities [1–12]. These phase-separated compartments allow rapid exchange of molecules from the surrounding environment [6, 13, 14]. Biological liquid-liquid phase separation (LLPS) of the nucleoli [10], Cajal body [11], and PML body in the nucleus and stress granules [1] in the cytoplasm have been shown to modulate a diverse and significant array of cellular functions. Most often, these phase-separated structures are spherical in shape (liquid

Jaladhar Mahato and Soumik Ray have been equally contributed to this chapter.

Andrzej Stanisław Cieplak (ed.), *Protein Aggregation: Methods and Protocols*, Methods in Molecular Biology, vol. 2551, https://doi.org/10.1007/978-1-0716-2597-2_27,

droplets) and dynamic entities that fuse upon contact [5]. In proteins, transient interactions (such as charged, cation-π, and hydrogen bonding) via low-complexity domains (LCDs) and intrinsically disordered regions (IDRs) are believed to drive LLPS [12, 15–17]. The cell regulates the expression levels of proteins in such a way that allows these droplets to form and redissolve whenever required [18].

However, abnormal regulation(s) and disease-associated condition(s) are often associated with the liquid-to-solid transition of LLPS, a phenomenon infamous for gradual rigidification of the phase-separated droplets. Although the liquid-to-solid transition could act as a necessary function [19], for most cases, it corroborates with toxic higher-order structure formation. In recent years, FUS [20, 21], tau [22, 23], TDP-43 [24], hnRNPA1 [15], and α-synuclein (*α*-Syn) [25] have been shown to undergo LLPS, which subsequently lead to aggregation of these proteins associated with various neurological disorders such as amyotrophic lateral sclerosis (ALS), Alzheimer's disease (AD), and Parkinson's disease (PD). This indeed has been clearly shown for *α*-Syn where phase-separated *α*-Syn droplets undergo a viscoelastic transition with time (from liquid-like to solid-like), which ultimately results in aggregation and amyloid fibril formation.

The primary sequence of natively unstructured *α*-Syn contains three distinct domains: the N-terminal domain, the non-amyloid β component (NAC) domain, and the flexible C-terminal domain [25]. The intermolecular interaction mediated through N-terminus and the NAC domain is primarily responsible for *α*-Syn LLPS and subsequent aggregation [25]. Bulk spectroscopic techniques provide ensemble-averaged information that can be very relevant, especially for homogeneous systems. However, rare events and specific molecular interactions within local domains of heterogeneous systems such as LLPS droplets are often obscured by dominant nonspecific interactions in solution. To understand intermolecular interaction exclusively inside the phase-separated droplets, microscopic methods are necessary, which selectively delineate information from spatially separated individual droplets.

Generally, the interaction (proximity) among the biomolecules is investigated by the conventional fluorescence co-localization method [26, 27]. In this method, the distinct biomolecules are tagged with different (colored) fluorophores, and each is imaged with the corresponding fluorescence channel. Here, the co-localized spatial region is a result of the coexistence of the relevant species, which are assumed to be interacting [26–29]. However, the spatial resolution of this co-localization is limited by the diffraction limit, which depends on the used radiation wavelength (λ) and the numerical aperture (NA) of the objective lens (resolution~$\lambda/2NA$). Typically, the diffraction limit for a microscope of high NA objective is ~200 nm [30]. It should be

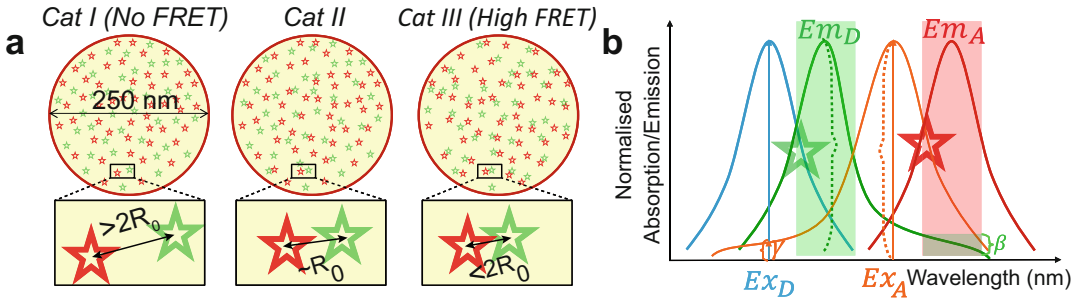

Fig. 1 (**a**) Schematic depiction of three different scenarios, which leads to the same co-localization in a diffraction-limited area. In *Category (Cat) I*, the *D* (green stars) and *A* (red stars) are randomly distributed, which is in contrast to *Cat III*, where the molecules are in close proximity due to the strong interaction and therefore would show *negligible* and *high* FRET, respectively. *Cat II* represents the situation where fractions of the *D* and *A* are engaged in molecular interaction, which results in *intermediate* FRET within a unit resolution area. *Cat II* may arise when most of the *D* and *A* are in intermediate distance compared to *Cat I* and *Cat III*. One *D* and *A* are zoomed in to highlight the proximity with respect to the Förster radius (R_0). (**b**) Typical absorption and emission profile of fluorophores used in practical FRET study showing the bleed-through (β) and cross talk (γ) along with their overlap of absorption and emission spectrum

noted that a volume of this dimension is much bigger than the size of molecules and can contain approximately a million probes in one unit resolution (diffraction-limited region) of a co-localized image. As a consequence, the fluorescence co-localization does not guarantee the interacting nature of biomolecules owing to the limited resolution of the fluorescence microscope (*see* **Note 1**) [26–30]. Figure 1a demonstrates this situation on a molecular scale with two kinds of biomolecules for three scenarios in a diffraction-limited area for the same number of molecules in each case. In *category I*, there is no interaction between the molecules, whereas in *category III*, most of the molecules strongly interact owing to close proximity. *Category II* represents the intermediate situation where a proportion of the molecules interact and the rest are randomly distributed. However, the fluorescence co-localization will show the co-localized emission (in a diffraction-limited area) for all these three different thought experiments where the extent of interactions is designed to be distinct.

In the context of visualization, it is important to ensure whether the probes are engaged in biomolecular interaction or not. This can be achieved if certain spectroscopic signatures corresponding to such interactions (or proximity) can be detected and spatially resolved. There are a few optical microscopy-based techniques to probe the interaction of dipoles within a diffraction-limited area, such as the interaction of proteins Bcl-2 and Beclin, and clustering of MHC class I molecules at the endoplasmic reticulum [31–33]. It is relevant to note that the detection of spectral signatures owing to dipole-dipole interaction is only observed when the interacting molecular species are within a distance of

nanometers from each other. This is because dipole-dipole interaction sharply falls off with distance (r), that is,$\propto \frac{1}{r^n}$, where $n \geq 3$ [34]. One of the consequences of commonly observed dipolar interactions between two chromophores is Förster resonance energy transfer (FRET), where radiationless transfer of energy occurs from a donor to acceptor [35]. This dipolar coupling between two molecules also depends on the overlap of the emission spectra of the donor (D) and the absorption spectra of the acceptor (A) [36]. Under situations when acceptors are emissive, energy migration from excited donors results in enhanced emission of the acceptors and simultaneous reduction of the donors' fluorescence quantum yield of the donors [33]. Thus, the sensitized emission from the acceptor in a donor-acceptor ($D - A$) system can be used as measure of FRET, because the extent of sensitization will scale with the efficiency of FRET. It should be noted that nonzero FRET efficiency can be detected only at short dipolar distances (~2–10 nm), although factors such as orientation of dipoles and medium can affect energy transfer [37]. Therefore, the fluorescence output due to FRET from two distinct probes can authenticate the interacting nature of the species, which enables FRET microscopy to be used for functional imaging.

Several FRET-based microscopy techniques have been developed to interrogate the biomolecular interaction, which provides answers to a large number of biological questions [38, 39]. In FRET microscopy, the sensitized emission is recorded along with the conventional D and A fluorescence channel (used in co-localization). The three distinct energetically separated channels are defined below based on their mode of excitation (Ex) and emission (Em):

$I_{Ex_D}^{Em_D} \rightarrow D$ channel fluorescence when excited at the donor (λ_{Ex_D}).
$I_{Ex_A}^{Em_A} \rightarrow A$ channel fluorescence when excited at the acceptor (λ_{Ex_A}).
$I_{Ex_D}^{Em_A} \rightarrow A$ channel fluorescence when excited at λ_{Ex_D}.

Each band of these channels is determined by the full width and half maxima (fwhm) of the emission peaks of D and A. In an ideal FRET microscopy experiment, the A channel intensity upon excitation of D, that is, $I_{Ex_D}^{Em_A}$, originates entirely from the sensitized emission. In such scenarios, the noticeable $I_{Ex_D}^{Em_A}$ indicates that the D and A undergo bimolecular interaction whereas negligible $I_{Ex_D}^{Em_A}$ points out to noninteracting species [40]. The magnitude of $I_{Ex_D}^{Em_A}$ determines the extent of interaction among the molecular species. However, it is relevant to note that $I_{Ex_D}^{Em_A}$ contain not only the sensitized emission but also the fluorescence from the cross-excitation of A when excited at absorption maxima of D (λ_{Ex_D}) as well as the leak-through of D emission in the A channel (*see* Fig. 1b) owing to broad spectral widths at room temperature. Therefore, even in the absence of FRET (i.e., no molecular interaction), $I_{Ex_D}^{Em_A}$

has contributions of fluorescence signals due to the cross talk (γ) from A and the bleed-through (β) from D [32, 35]. Removal of the cross talk $\left(\gamma I_{Ex_A}^{Em_A}\right)$ and bleed-through $\left(\beta I_{Ex_D}^{Em_D}\right)$ contributions from the $I_{Ex_D}^{Em_A}$ can be used to estimate the maximum intensity enhancement due to the sensitized emission (SE) of the acceptor in the FRET pair (*see* **Note 2**):

$$SE = I_{Ex_D}^{Em_A} - \gamma I_{Ex_A}^{Em_A} - \beta I_{Ex_D}^{Em_D}$$

The sensitized emission can be normalized to obtain the apparent sensitization efficiency (ASE) (*see* **Note 3**). The calculation of ASE in each pixel in a fluorescence image will, therefore, provide the spatially resolved map of FRET and thereby the spatial variation of biomolecular interactions (*see* **Note 4**).

While probing the bimolecular interaction using the existing intensity image-based FRET microscopy method, it is important to address several technical issues. First, the fluorescence detection channels collect photons through energetically separated band-pass filters. However, it is extremely challenging to match pairs of band-pass filters with the emission spectral characteristics of the donor and acceptors. This, combined with detrimental effects like polarization and chromatic aberration, poses difficulty in accurately determining the bleed-through contributions. Besides, for microscopic structures, the collection of absorption spectra from donors and acceptors is extremely challenging due to weak signals, uncertain path length, and the variation of local concentrations. In effect, the number of *Ds* and *As* that contribute to the emission within a diffraction-limited area remains uncertain, and thus, the interpretation of sensitized/FRET signal becomes ambiguous, especially when D and A chromophores are not covalently connected. Finally, any small changes of spectral envelopes under specific conditions or environments in the $D - A$ system during experiments would yield spurious results, owing to the range of existing channels not being calibrated for such spectral profiles. Therefore, ideally, the results from two such sets of experiments should not be compared. It is relevant to mention here that single-molecule FRET experiments, such as alternating-laser excitation (ALEX) FRET, bypass several of these factors; however, the technique cannot be extended to a system where the number of D and A is much higher [41].

This chapter describes a spectrally resolved FRET (SR-FRET) microscopy method via the collection of spatially resolved emission spectra of non-covalent assembly of donors' and acceptors' $D - A$ system, to obtain the enhancement in (sensitized) emission owing to an energy transfer from the D to A. The proof of principle has been demonstrated on the site-specific phase-separated droplets of 74C-α-Syn during its LLPS and subsequent liquid-to-solid transition. The fluorescent probes (fluorescein-5-maleimide (D) and rhodamine-C2-maleimide (A)) were attached to the 74th cysteine

to probe the NAC region of α-Syn (~65–95 amino acids) during LLPS (*see* **Note 5**). It is relevant to mention that one can judicially choose different FRET pairs to avoid the drastic correction which might arise from the cross talk $\left(\gamma I_{Ex_A}^{Em_A}\right)$ and bleed-through $\left(\beta I_{Ex_D}^{Em_D}\right)$ (*see* **Note 6**). The SR-FRET microscopy records the entire emission spectrum from the individual particle (collection of molecules) or in this case liquid droplets, in a single shot. As the results are spectrally resolved, the extraction of γ and β (from pure D and A) is simple (*see* Fig. 2a, b) which in turn helps easy estimation of the possible maximum emission intensity from a $D-A$ system without FRET (*see* Fig. 2c). The details have been described in Subheading 3.8. To investigate the biomolecular interactions in system of interest, the spectrum is recorded at λ_{Ex_D}, which is used to obtain the intensity for both the direct emission from D (peak of $I_{Ex_D}^{Em_D}(\lambda)$) and the sensitized emission (see blue profile in Fig. 2d,e). On the other hand, the emission intensity only from A molecules (peak of $I_{Ex_A}^{Em_A}(\lambda)$) in $D-A$ is obtained from the emission spectrum for λ_{Ex_A} (see red dotted profile in Fig. 2d, e). The method does not use filters to separate the donor, acceptor, and sensitized emission. It should be emphasized that the extracting *true* FRET efficiency is challenging due to the lack of information on the absolute number of D and A. The method described here provides an alternate route for such systems to compare and to quantify the progressive change of intermolecular interactions (see Fig. 2d, e) in individual microscopic objects. It is worth mentioning that this technique can be employed to study structural and functional aspects of a variety of self-assembled soft materials; these include sub-diffraction-limited polymersomes, which have phase-separated donors and acceptors [42] and supramolecular block copolymers containing alternate donor and acceptor segments [43] to investigate energy migration over mesoscale (>500 nm) distances.

2 Materials

2.1 74C-α-Syn Expression and Purification

1. *E. coli* BL21 (DE3)-competent cells
2. pRK172 plasmids cloned with Cys-74C-α-Syn [25]
3. QuikChange Site-Directed Mutagenesis Kit *(Stratagene, La Jolla, CA)*
4. 1 mM isopropyl-β-D-thiogalactoside (IPTG)
5. 1 mM dithiothreitol (DTT)
6. Protease inhibitor cocktail (Roche Applied Science, USA)

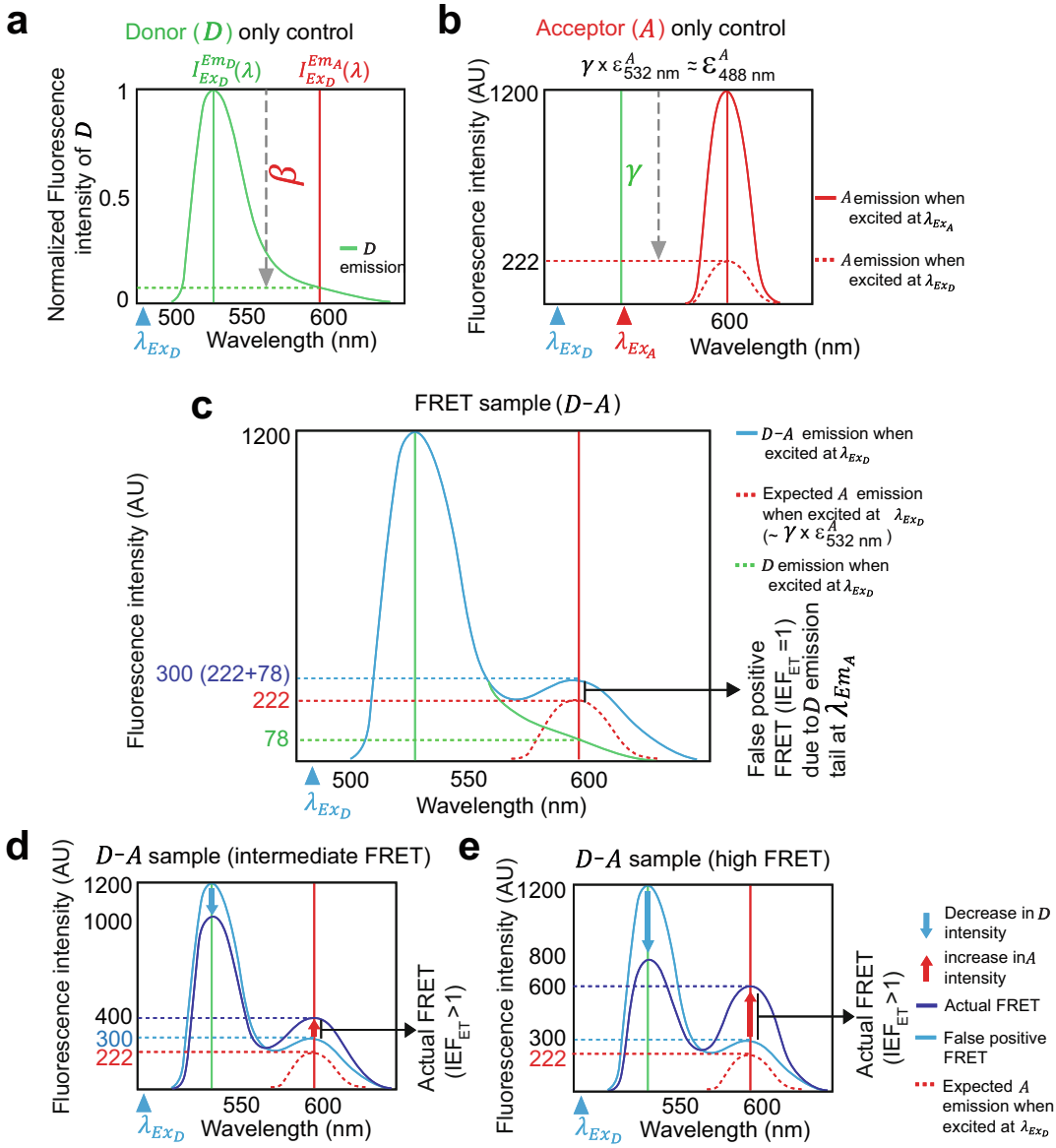

Fig. 2 Schematic representation of the SR-FRET concept and the procedure for β and γ correction. (**a**) Diagram showing emission spectrum from a *D*-labeled 74C-α-Syn (*D* control) droplet at λ_{Ex_D}. This spectrum is normalized to 1 to estimate the contribution of *D* at λ_{Em_A}, which is the bleed-through (β) factor. (**b**) Schematic of an emission spectrum of a *A*-labeled 74C-α-Syn droplet (*A* control) at λ_{Ex_D} and λ_{Ex_A}. The ratio of fluorescence intensity at the emission peak of A $\left(i.e., \lambda_{Em_A}^{max}\right)$ at λ_{Ex_D} with the fluorescence intensity at λ_{Ex_D}, provides the cross talk (γ) factor. (**c**) Representation of an emission profile of a droplet containing both *D*- and *A*-labeled 74C-α-Syn at λ_{Ex_D}. Here, the *A* peak intensity is higher than *A* alone (control) in the absence of FRET because the fluorescence intensity arises from the tail of *D* at λ_{Em_A} defined as false-positive FRET. (**d**) A true positive FRET scenario is observed in $D-A$ sample when the *A* peak intensity at $\lambda_{Em_A}^{max}$ is higher than *A*-only control (γ corrected) even after correction of tail contribution (β). Note that the *D* intensity at $\lambda_{Em_D}^{max}$ decreased due to energy transfer. (**e**) The *A* peak intensity increases significantly for a higher FRET scenario, and the *D* peak intensity decreases further. (This schematic is reproduced from article [25] with permission from Springer Nature)

7. Lysis buffer: 50 mM Tris-HCl, pH 8.0, 10 mM trypsin-ethylenediaminetetraacetic acid (EDTA), 150 mM NaCl, and protease inhibitor cocktail
8. 10% (w/v) streptomycin sulfate
9. Glacial acetic acid
10. Saturated ice-cold ammonium sulfate (at 4 °C) and absolute ethanol
11. 100 mM ice-cold ammonium acetate (at 4 °C)
12. BOD shaker incubator (37 °C)
13. Centrifuge (up to 13,000 rpm)
14. Probe sonicator (Sonics & Materials, Inc, USA)
15. Lyophilizer

2.2 Low-Molecular-Weight (LMW) α-Syn

Dialysis of α-Syn-lyophilized powder against desired buffer may lead to formation of higher-order assembly because α-Syn is very prone to aggregation. Therefore, it is recommended to centrifuge α-Syn after dialysis through a 100 kDa cutoff membrane filter and collect the flow-through. The membrane retains higher-order structures (if any) and allows only low-molecular-weight (LMW, monomeric) α-Syn to pass (see Subheading 3.2):

1. 100 mM sodium phosphate buffer stock: 3.1 g NaH_2PO_4. H_2O, 10.9 g Na_2HPO_4, 1 L of Milli-Q water, and pH adjusted to 7.4 with NaOH/HCl. Store at 4 °C. It is advisable to add 0.01% sodium azide to the sodium phosphate buffer solution to prevent bacterial/fungal contamination. 20 mM sodium phosphate buffer, pH 7.4, is obtained by adding four volumes of Milli-Q water to one volume of stock solution. Check the pH after dilution and filter the buffer using a 0.22 μm membrane.
2. Lyophilized 74C-*α*-Syn powder.
3. Centrifuge (at least 13,000 rpm) with temperature control (4 °C).
4. pH meter.
5. 10 kDa cutoff membrane, 100 kDa cutoff filters, and 0.22 μm membrane filters.
6. UV-Vis spectrophotometer.

2.3 Fluorescent Labeling of α-Synuclein and Subsequent LLPS of the Labeled Proteins

1. 500 μM LMW 74C-*α*-Syn stock in 20 mM phosphate buffer pH=7.4: ~25–30 mg lyophilized 74C-*α*-Syn powder, 500 μL 20 mM sodium phosphate buffer pH 7.4, and 0.01% sodium azide (*see* **Note 7**).
2. Dimethyl sulfoxide (DMSO).

3. Fluorescein-5-maleimide (*D*) stock: Prepare a 10 mM stock of fluorescein-5-maleimide in DMSO.
4. Rhodamine-C2-maleimide (*A*) stock: Prepare a 10 mM stock of rhodamine-C2-maleimide in DMSO.
5. Polyethylene glycol (PEG)-8000 stock: 3 g PEG-8000 powder and 10 mL 20 mM sodium phosphate buffer pH 7.4.
6. Micro-pH meter probe.
7. Dialysis units: 10 kDa dialysis bag and 100 kDa molecular weight cutoff filter.
8. UV/Vis spectrophotometer.
9. Magnetic stirrer unit with magnetic beads (7 × 2 mm).
10. Glass slides and coverslips.

2.4 Microscopy Setup for FRET Measurement

1. Inverted microscope (we used Nikon Eclipse TE2000-U)
2. Two main laser sources: $\lambda_{Ex_D} = 488$ nm (we used OXXIUS, model: ACX-CTRB) and $\lambda_{Ex_A} = 532$ nm (we used LASER-GLOW, model: LRS-0532-PFM-00200-03). Two more radiation sources (405 nm and 633 nm):
3. Neutral density filters and a $\lambda/4$ wave plate
4. Objective lens (we used Nikon, Oil immersion, 1.49 NA, 60X, Apo TIRF)
5. Glass slides and coverslips (we used Blue Star, India)
6. Filters: Two bandpasses (515–565 nm and 590–700 nm), one long pass (500–700)
7. Relay lens: A combination of two plano-convex (f=*65mm*)
8. Polychromator: Combination of an adjustable slit and a transmission grating (70 grooves/mm (*see* **Note 8**)
9. Array detector: sCMOS camera (we used Hamamatsu ORCA-Flash 4.0 V3)
10. Data acquisition software: Micromanager
11. Image analysis software: ImageJ (NIH)
12. Data analysis: Origin Pro 8 and MATLAB 2019a (*see* **Note 9**)

3 Methods

3.1 74C-α-Syn Expression and Purification

The single Cys mutant (V74C) was a kind gift from Prof. Roland Riek, ETH Zurich, Switzerland, and was generated with QuikChange Site-Directed Mutagenesis Kit (Stratagene, La Jolla, CA). The vector pRK172 was also a kind gift from Prof. Roland Riek, ETH Zurich, Switzerland:

1. Transform the *E. coli* BL21 (DE3)-competent cells with the desired plasmid. Add 1 mM IPTG to induce the transformation process for 4 h at 37 °C.
2. Pellet down the *E. coli* at 4000 rpm, 4 °C, for 30 min.
3. Resuspend the pellet using lysis buffer. Add 0.01% sodium azide to the buffer solution to prevent bacterial/fungal contamination.
4. To prevent the proteolytic cleavage, add protease inhibitor cocktail.
5. Lysed the cells by probe sonicator at 40% amplitude with pulse 3 s on and 1 s off for 10 min (on ice or at 4 °C).
6. Denature the suspension for 20 min using a hot water bath (at 95 °C).
7. Collect the supernatant after centrifugation at 10,000 rpm for 30 min at 4 °C.
8. Precipitate DNA from the supernatant using ~2 mL/ L streptomycin sulfate (10% (w/v) and glacial acetic acid.
9. Collect the supernatant after discarding the DNA by centrifugation at 10,000 rpm for 30 min.
10. Precipitate the supernatant at 4 °C overnight using an equal volume of saturated ammonium sulfate.
11. Subsequently, centrifuge the solution twice at 12,000 rpm at 4 °C for 45 min to pellet down the protein.
12. Dissolve the pellet in 50% ammonium sulfate and centrifuge at 12,000 rpm at 4 °C for 45 min.
13. Resuspend the precipitate thrice by 100 mM ammonium acetate. Add an equal volume of ethanol to the suspension to precipitate the α-Syn for 30 min at room temperature (25 °C).
14. Dissolve the final pellet protein with a minimum volume of 100 mM ammonium acetate, flash-frozen with liquid nitrogen and lyophilized.
15. Check the purity of the protein by running SDS-PAGE or MALDI/TOF.
16. For Cys mutants of α-Syn, 1 mM DTT must be added during the purification steps to avoid intermolecular disulfide linkages [25].

3.2 Aggregate-Free, Low-Molecular-Weight (LMW) 74C-α-Syn Preparation

1. Dissolve ~25–30 mg of lyophilized 74C-α-Syn in ~500 μL of 20 mM sodium phosphate buffer (pH 7.4) to prepare the primary protein stock solution.
2. Adjust the pH of the solution to 7.4 using a pH meter.
3. Activate 10 kDa dialysis membranes by stirring them in boiling water with gentle rubbing for 15 min.

4. Dialyze the protein solution for 10–12 h at 4 °C against 20 mM phosphate buffer (7.4) using the 10 kDa cutoff membrane.
5. Pre-equilibrate 100 kDa cutoff filters with 20 mM phosphate buffer (7.4). Add ~300 μL of 20 mM phosphate buffer (pH 7.4) to the filter, and centrifuge at 6000 rpm for 15 min at 4 °C. Repeat this step three times.
6. Centrifuge the solution at 13000 rpm for 30 min at 4 °C.
7. Take out the supernatant and pass through the equilibrated 100 kDa cutoff filter by centrifugation at 10,000 rpm for 30 min at 4 °C.
8. Collect the flow-through and measure the 280 nm absorbance for estimation of the protein concentration of the LMW 74C-*α*-Syn using a UV/Vis spectrophotometer (*see* **Note 10**).

3.3 Fluorescent Tagging and LLPS of Labeled α-Syn

1. Prepare reaction mixtures containing 500 μM of the LMW 74C-*α*-Syn and 2.5 mM (5-mole excess) of fluorescein-5-maleimide and rhodamine-C2-maleimide separately. Mix the constituents of the reaction mixture for 2h at 25 °C with the help of a micro-stirrer bead (7 mm × 2 mm) with very slow rotation (~20 rpm) on a magnetic stirrer. This will allow the protein molecules to get attached to the fluorescent molecule (s) specifically at the 74th cysteine.
2. Remove the excess dye by dialysis against 20 mM phosphate buffer, pH 7.4 (for ~48 h with changing of the buffer every 5 h) using an activated 10 kDa dialysis membrane at 4°C (see Subheading 3.2).
3. Prepare a stock LMW solution of 500 μM of unlabeled and fluorescently labeled 74C-*α*-Syn by mixing one volume of labeled 74C-*α*-Syn (500 μM) and nine volumes of unlabeled 74C-*α*-Syn (500 μM). This will serve as the master stock to prepare subsequent LLPS mixtures. In the master stock, the protein is now 10% labeled (90% unlabeled).
4. From the master stocks (in **step 3**), prepare the LLPS reaction mixtures for both fluorescein-5-maleimide (green)- and rhodamine-C2-maleimide (red)-tagged 74C-*α*-Syn in separate reaction tubes. In the LLPS reaction mixture, the protein concentration will be 200 μM in the presence of 10% (w/v) PEG-8000 (prepared in 20 mM sodium phosphate buffer, pH 7.4).
5. Mix equal volume of the LLPS reaction mixture (in **step 4**) containing fluorescein-5-maleimide-labeled and rhodamine-labeled 74C-*α*-Syn. This will be the FRET solution where both the donor (fluorescein-5-maleimide-labeled 74C-*α*-Syn) and the acceptor (rhodamine-C2-maleimide-labeled 74C-*α*-Syn) are present in equal proportions (concentration as well as volume).

6. Prepare the donor-only control LLPS reaction mixture from the master stock of fluorescein-5-maleimide-labeled 74C-α-Syn (in **step 3**). This reaction mix will have 200 μM 10% (v/v) fluorescein-5-maleimide-labeled 74C-α-Syn in the presence of 10% (w/v) PEG-8000 (prepared in 20 mM sodium phosphate buffer).
7. Prepare the acceptor-only control LLPS reaction mixture from the master stock of rhodamine C2-maleimide-labeled 74C-α-Syn (in **step 3**). This reaction mix will have 200 μM 10% (v/v) rhodamine C2-maleimide-labeled 74C-α-Syn in the presence of 10% (w/v) PEG-8000 (prepared in 20 mM sodium phosphate buffer) (*see* **Note 11**).
8. Drop-cast 15–20 μL of the mixture onto a glass slide and sandwich the solution with 12 mm coverslips. Seal the sides of the coverslip with commercially available nail polish for making the chamber airtight.
9. Prepare a moist chamber by making a water-soaked tissue paper bed in a box.
10. Put the slides in the moist chamber and airtight the chamber.
11. Incubate the chamber containing the samples in 37 °C.
12. In such conditions, 74C-α-Syn would undergo LLPS after 48 h (two days). Put the phase-separated droplets under microscopy-based FRET studies at regular time intervals starting from day 2.

3.4 Spectrally Resolved FRET (SR-FRET) Microscopy

The method employed here requires the modification of an existing inverted optical microscope in the detection mode. However, we describe the entire alignment of the microscopy setup as many subtle details have to be maintained while performing the experiments. The modification has been done on a wide-field epi-/total internal reflection fluorescence (TIRF) microscope. The humidity must be controlled on the sample chamber or in the microscopy room to prevent sample drying due to the evaporation. The details of instrument alignment are depicted in Fig. 3a and provided below:

1. *Excitation:* Align the two laser lines ($\lambda_{Ex_D} = 488$ nm; $\lambda_{Ex_A} = 532$ nm) and focus on the back focal plane of the objective. Maintain the identical power density ($5 \mathrm{Wcm}^{-2}$) of the two excitation sources with the help of a power meter (*see* **Note 12**). A set of ND filters can help to maintain equal power. Place a broadband $\lambda/4$ plate to get rid of the polarization artifact due to the photo-selection.
2. *Illumination*: Place the sample on the stage so that the coverslip part touches the microscope stage, and the glass slide part is at the top side (*see* **Note 13**). Illuminate the sample with a high

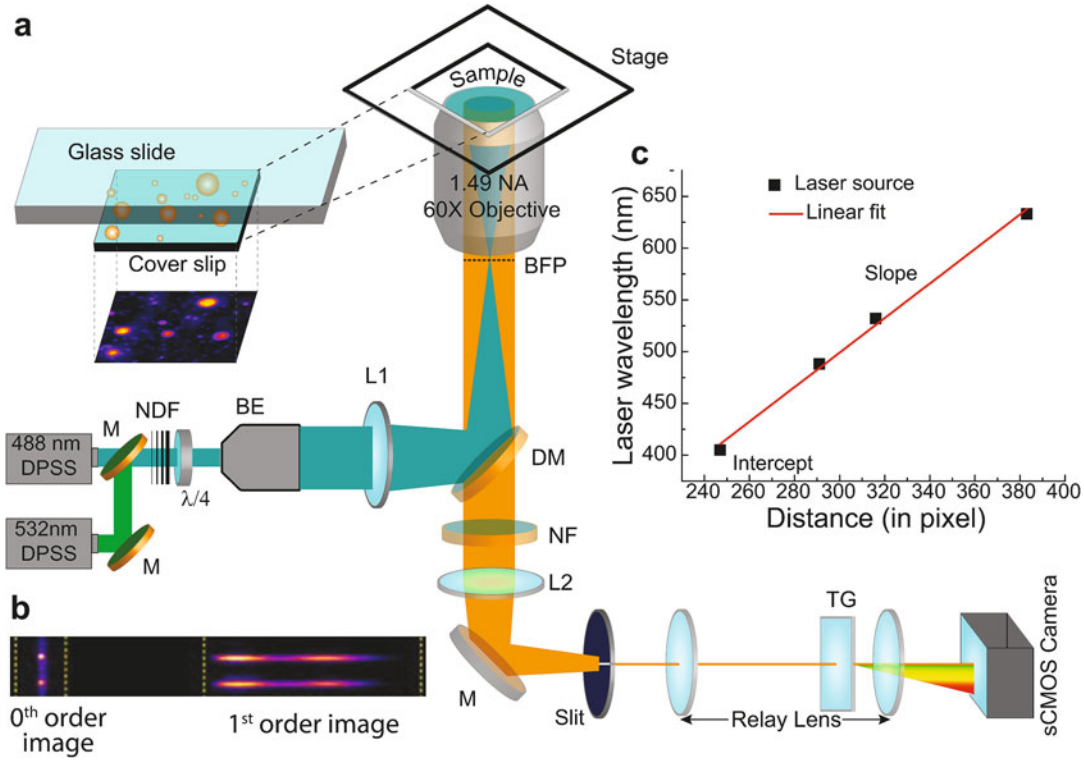

Fig. 3 (**a**) The layout of spectrally-resolved FRET microscopy. The shorthand notation used in the figures carries the following meaning – NDF→ neutral density filter,$\lambda/4$ → quarter-wave plate, BE→ beam expander, L1 and L2→ lenses, DM→ dichroic mirror, BFP→ back focal plane, M→ mirror/prism, and TG→ transmission grating. Here, both the zeroth-order and the first-order images fall on the same array detector. It should be pointed out that the $I_{Ex_D}^{Em_D}$, $I_{Ex_D}^{Em_A}$, and $I_{Ex_A}^{Em_A}$ images can be recorded in the same setup if slit and TG are removed, and appropriate band-pass filters are used. (**b**) The typical spectral image from $D - A$ sample showing the zeroth- and first-order image (reproduced from article [42], at Fig. SI15 with permission from the American Chemical Society). (e) Calibration of sCMOS array detector forms pixel distance to wavelength (nm)

NA objective lens. Maintain the uniformity of the field; a beam expander at the excitation part can help to achieve this.

3. *Detection:* Keep appropriate dichroic mirror and notch filters after the objective, which collects the emission from the sample. Mount a narrow slit at the first image plane (*see* **Note 14**). Make a second image plane at the array detector by using a relay lens after the slit. Place a transmission grating (TG) inside the relay tens such that its zeroth-order and first-order image is formed in the same array detector (*see* **Note 15** and Fig. 3b). Open the slit such that its open dimension becomes not more than diffraction limit (*see* **Note 16**). Make sure the data acquisition software function properly.

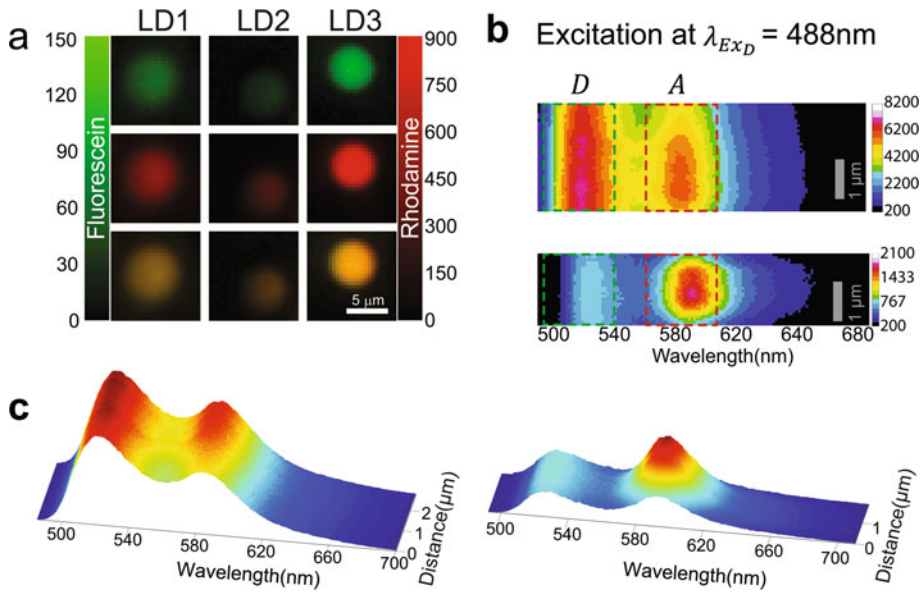

Fig. 4 (**a**) Mixture of fluorescein-5-maleimide-labeled 74C-α-Syn (*D*) and rhodamine-C2-maleimide-labeled 74C-α-Syn (*A*) liquid droplets represented by green and red colors, respectively, along with their co-localized image. (**b**) Typical, spectral images of a single phase-separated droplet containing both *D*- and *A*-labeled 74C-α-Syn proteins when excited at λ_{Ex_D} at d2 (top) and d7 (bottom). Two distinguished spectrally resolved domains for *D* and *A* have been marked by dotted line box. (**c**) Three-dimensional rendition of intensity profiles of the spectral image from the two individual droplets, as shown in Fig. 4b, shows two emission peaks for *D* and *A* emissions. These plots could provide information on the spatial heterogeneity within a droplet. Note that the fluorescence maximum at *A* relative to *D* is more for the second droplet. (Figure 4a is reproduced from article [25] with permission from Springer Nature)

3.5 Prior Check Before SR-FRET Measurements

It is imperative to check whether the fluorescently tagged 74C-α-Syn sample undergoes liquid-liquid phase separation or not before performing SR-FRET. Figure 4a shows that the $D - A$ system forms phase-separated spherical liquid droplets (the data for only D and A are not shown). Besides, the co-localized emission from D and A in $D - A$ is readily observable, which indicated the possibility of interaction among the protein molecules. It has been observed that protein aggregates emerge from α-Syn droplets after 20 days of maturation, and after 30 days, the LLPS transformed into a hydrogel [25]. Meanwhile, the imaging setup has been turned on for the spectral imaging of phase-separated droplets.

3.6 Collection of SR-FRET Microscopy Data

The following step will guide to perform a complete set of SR-FRET experiments. Here, we take SR-FRET data at d2, d7, and d24 time points. Collect at least 50 spectral images for each set of experiments. All the experiments have been performed 1 h after the coverslips have been placed on the stage (*see* **Note 17**). The sample has been taken from the microscope and stored for

maturation till the next time points. Typically, spectral images of labeled 74C-α-Syn droplets were collected at 300 ms exposure, and the temperature was maintained at 25 °C:

1. Day 2: Record the spectral images of several spatially separated individual droplets containing only D at $\lambda_{Ex_D} = 488$ nm.
2. Day 2: Record the spectral images of several spatially separated individual droplets containing only A at $\lambda_{Ex_A} = 532$ nm . Immediately, collect another spectral image of the same area, however at $\lambda_{Ex_D} = 488$ nm.
3. Day 2: Record spectral image of a droplet containing both the donor- and acceptor-labeled proteins upon excitation at $\lambda_{Ex_A} = 532$ nm. Record another spectral image of the same droplet at $\lambda_{Ex_D} = 488\ nm$ of the same area (*see* **Note 18**).
4. Day 2: Record the zeroth- and first-order spectra of four laser line sources (405 nm, 488 nm, 532 nm, and 633 nm) to calibrate the wavelength from pixels to nm (*see* **Note 19**).
5. Day 7: Place the same LLPS sample (which was imaged on d2) on the microscope stage, and repeat **steps 1–4** to obtain the spectral image (*see* **Note 20**).
6. Day 24: Mount the sandwiched coverslips containing LLPS sample, which were imaged at d7 on the microscope. Collect several spectral images from each set of experiments as directed by **steps 1–4**.

3.7 Spectral Image Calibration

The experiments to collect the spectral image have been performed, as outlined in Subheading 3.6. The calibration procedure of SR-FRET data differs from the intensity image-based FRET microscopy. Figure 3c shows the calibration of the spectral image from distance in pixels to wavelength (nm), and each step has been described in the following section. Two such representative images from phase-separated $D - A$ droplet have been shown in Fig. 4b along with its surface plot in Fig. 4c when excited at λ_{Ex_D}. The appearance of two peaks corresponding to the D and A emissions is evident for these droplets. In addition, the A emission intensity relative to the D emission is higher for the second droplet collected at d7 than the first one collected at d2. It should be noted that the extracted spectral profile has been integrated over those pixels of a droplet, which has been selected by the slit, and thereby, the spectra are spatially averaged for a single droplet. However, our method of collecting spatially resolved fluorescence spectra (*see* Fig. 4b–c) could allow for monitoring the spatial distribution of sensitization efficiency or the apparent FRET efficiency within a single phase-separated liquid droplet provided that the droplets are reasonably large (several microns). It should be mentioned that the results collected on different days cannot be compared without proper calibration on each day:

1. Open a spectral image in a visualization software (such as ImageJ) and find a liquid protein droplet in it. Select an ROI containing the droplet from the center of the zeroth-order image to the far end of its corresponding the first-order dispersed image.
2. Draw the line profile of the selected ROI. The x-axis is the wavelength in pixel, and the y-axis contains the fluorescence count. Export the data to a computer program that can display data and perform arithmetic calculations (Origin 8).
3. Collect the line profile from the top and bottom part of the existing ROI, which has three-pixel breadth. Calculate the average line profile. Subtract the average line profile from the profile containing the droplet (*see* **Note 21**).
4. Extract the line profile from the four laser sources, that is, 405 nm, 488 nm, 532 nm, and 633 nm. Estimate the distance from first-order peak maxima to the zeroth-order peak for all the four lasers. Plot the wavelength in the y-axis and pixel distance on the x-axis. Calculate the slope and intercept with the linear fitting of this plot (*see* Fig. 2c).
5. Replace the x-axis of the droplet's spectral profile with the extracted slope and intercept (*see* **Note 22**).

3.8 Quantification of Sensitization Efficiency

The spectral profile of droplets has been extracted using the step, as mentioned in Subheading 3.7. The emission spectrum from the droplet containing the only donor fluorescein-5-maleimide (D)- and only acceptor rhodamine-C2-maleimide (A)-labeled 74C-α-Syn has a peak at 530nm (λ_{Em_D}) and 595nm(λ_{Em_A}) . The peak intensities have been compared to compute the intensity enhancement factor due to energy transfer (IEF_{ET}) or the apparent FRET efficiency. Here, we have analyzed only the spatially averaged emission spectra over a single droplet. The steps associated with the calculation of IEF_{ET}/apparent FRET efficiency are schematically presented in Fig. 2. The results of this analysis have been shown in Fig. 5 for five representative single droplets at d2, d7, and d24. The variation of IEF_{ET} at a particular day for different droplets has been noticed each day, as shown in Fig. 5a–c. The average profile of IEF_{ET} has been computed to compare with the data collected on a different day, which has been shown as a thick orange profile in Fig. 5a–c. The evolution of IEF_{ET} with the incubation time is shown in Fig. 5d, which reveals gradual increment of IEF_{ET} with time (days). The increase in IEF_{ET} with incubation time indicates either the progressive enhancement of proximity among 74C-α-Syn proteins or gradual increase of number 74C-α-Syn molecules in the phase-separated protein pools during the maturation of the phase-separated protein. The following are the steps to quantify the sensitization efficiency (or the apparent FRET efficiency):

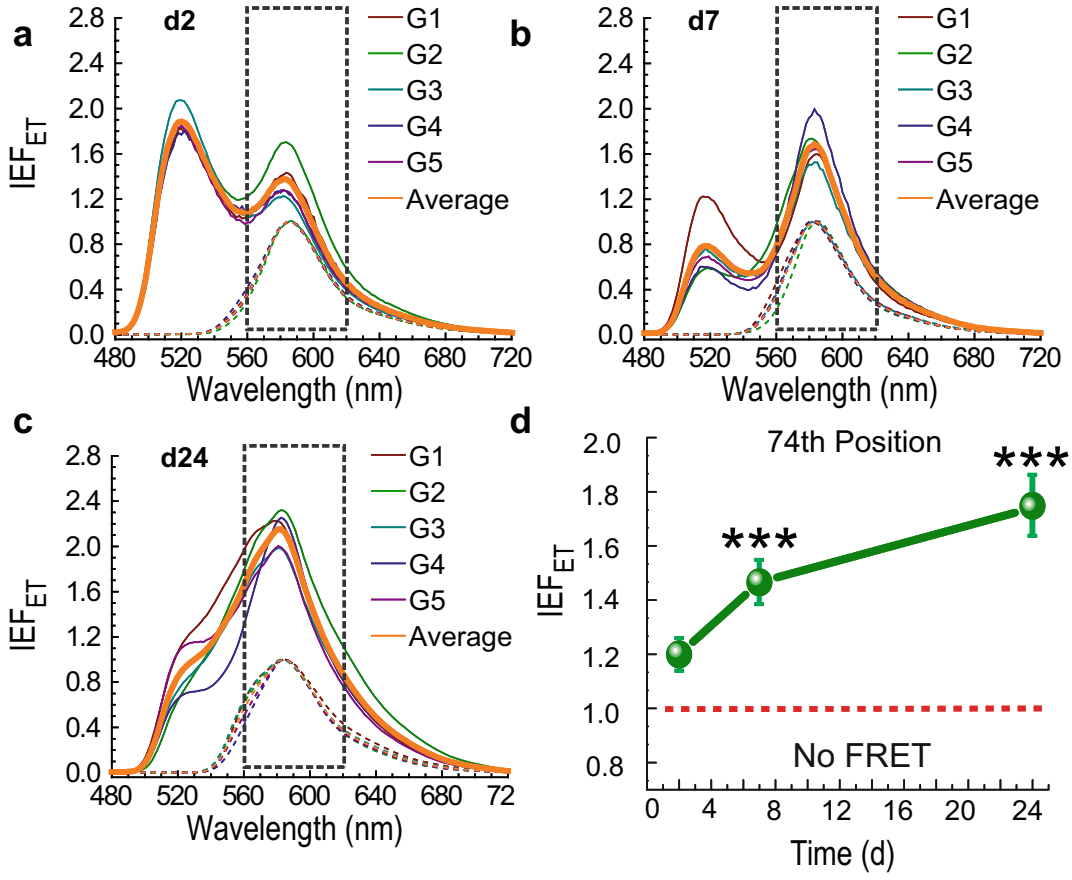

Fig. 5 IEF_{ET} plot of five representative $D - A$-tagged 74C-α-Syn phase-separated droplets at (**a**) d2, (**b**) d7, and (**c**) d24 presented in the emission spectral profile of $D - A$, which has been normalized with the false-positive FRET (*see* **Note 25**). Note that the y-axis applies to the dotted square area and should not be interpreted with the D spectral profile. The variation of IEF_{ET} among the droplets on a particular day is very evident. The thick orange spectrum is the average of these five spectra. A gradual increase in average IEF_{ET} with time (days) has been observed for such $D - A$-tagged 74C-α-Syn phase-separated droplets. (**d**) The progressive enhancement of IEF_{ET} with time (day) for 74C-α-Syn droplet indicates the gradual increase of proximity for 74C-α-Syn droplet molecules, or more number of 74C-α-Syn interacts inside the droplets during the maturation of the phase-separated protein droplets (*see* **Note 26**). The P values (***$P \leq 0.001$) were determined using a one-way ANOVA followed by a Student-Newman-Keuls post hoc test with a 95% confidence interval. (This figure is reproduced from article [25] with permission from Springer Nature)

1. Open spectral image of a droplet containing the only D that has been excited at $\lambda_{Ex_D} = 488\ nm$. Extract spectral line profile of that droplet. Repeat the same for several droplets. Normalize the emission spectra between 0 and 1 (*see* **Note 23**). Calculate the β from the following equation:

$$\beta = \frac{I^{Em_A}_{Ex_D}(\lambda)}{I^{Em_D}_{Ex_D}(\lambda)}, \text{ from droplets only } D \text{ molecules}$$

2. Extract spectral line profile of droplet that has been tagged with the only A and excited at $\lambda_{Ex_A} = 532$ nm. Extract the spectral line profile from the same area when excited at donor, that is, $\lambda_{Ex_D} = 488$ nm. Select more droplets and extract the spectra at both $\lambda_{Ex_A} = 532$ nm and $\lambda_{Ex_D} = 488$ nm. Estimate the γ factor (*see* **Note 24**):

$$\gamma = \frac{I_{Ex_D}^{Em_A}(\lambda)}{I_{Ex_A}^{Em_A}(\lambda)}, \text{ from droplets of only } A \text{ molecules}$$

3. Open the spectral image of droplets containing both the donor and acceptor that has been excited at $\lambda_{Ex_D} = 488$ nm. Extract the spectral line profile from one droplet by selecting an appropriate ROI. Open the spectral image of the same area which has been excited at $\lambda_{Ex_A} = 532$ nm. Extract the spectral line profile of the same droplet from the same ROI.
4. Multipy the acceptor emission spectrum which was obtained when $D - A$ sample was excited at $\lambda_{Ex_A} = 532$ nm with the γ factor.
5. Multiply the donor peak maxima which were obtained when $D - A$ sample was excited at $\lambda_{Ex_D} = 488$ nm with the normalized emission spectra of fluorescein-5-maleimide-labeled 74C-α-Syn.
6. Add the spectrum obtained in **steps 4** and **5**. This is the spectrum without energy transfer for a $D - A$ sample (see **Note 25**).
7. Calculate the intensity enhancement factor due to the energy transfer IEF_{ET}, the enhancement of intensity (in $I_{Ex_D}^{Em_A}$) due to the sensitization with respect to in the absence of energy transfer (*see* **Note 26** and **Note 27**):

$$IEF_{ET} = \frac{I_{Ex_D}^{Em_A}}{\left[\beta \times I_{Ex_D}^{Em_D}(\lambda) + \gamma \times I_{Ex_A}^{Em_A}(\lambda)\right]}$$

4 Notes

1. The super-resolved fluorescence microscopy, such as PALM, STORM, and STED, is not diffraction-limited, and its spatial resolution is ten times higher, that is, 20 nm [44, 45]. The two-color super-resolved image can distinguish *Cat I/Cat II/Cat III* with improved precision. However, still, the subtle change of molecular interaction (proximity) over time cannot be monitored as the ~20 nm is quite high to the dimension of molecules.

2. Generally, for most practical FRET pair, the donor gets hardly excited at λ_{Ex_A}, that is, the cross talk contribution from the donor is negligible.
3. The apparent sensitization efficiency (*ASE*) can be expressed using the following formula:

$$\mathrm{ASE} = \frac{\text{sensitized intensity}}{\text{total donor intensity}} = \frac{\left(I_{Ex_D}^{Em_A} - \beta I_{Ex_D}^{Em_D} - \gamma I_{Ex_A}^{Em_A}\right)}{I_{Ex_D}^{Em_D} + \left(I_{Ex_D}^{Em_A} - \beta I_{Ex_D}^{Em_D} - \gamma I_{Ex_A}^{Em_A}\right)}$$

4. The *ASE* image where structural features are absent will be dominated by background intensity and is almost equal for $I_{Ex_D}^{Em_A}$, $I_{Ex_D}^{Em_D}$, and $I_{Ex_A}^{Em_A}$. This aspect should be remembered while interpreting the obtained result.
5. Cysteine labeling does not affect protein structure nor LLPS behavior.
6. One might choose *D* and *A* in such a way that the excitation spectrum of the *D* does not overlap with the excitation spectrum of the acceptor (cross talk). Also, emission spectrum of the *D* should not overlap with emission spectrum of *A* to avoid corrections for bleed-through. However, bleed-through or cross talk is unavoidable when there are a disproportionate number of donors and acceptors in an assembly where FRET is being probed [42].
7. Add a few drops of 2(N) NaOH if the powder does not dissolve properly.
8. We used 70 grooves/mm TG from optometric; however, 300 grooves/mm gratings can also be used for higher resolution if there is enough signal.
9. A computer program which can simultaneously display a 16-bit image and perform arithmetic calculation such as MATLAB is enough to complete the data analysis.
10. The molar extinction coefficient (ε) used for calculating concentration is of 5960 $M^{-1}cm^{-1}$ for 74C-α-Syn.
11. The control sets of experiments are performed to extract the β and γ, respectively, from D- and A-labeled 74C-α-Syn.
12. It is essential to maintain the identical power for $\lambda_{Ex_D} = 488$ nm and $\lambda_{Ex_A} = 532$ nm. Our calculation of IET_{ET} is based on these criteria. This is because in a $D - A$ sample, λ_{Ex_A} only excite the *A*, and hence the emissions are from *A* molecules; however, λ_{Ex_D} excite both *D* and *A* molecules. The multiplication of β with the $I_{Ex_A}^{Em_A}(\lambda)$ will provide the expected intensity from only *A* molecules if excited at λ_{Ex_D} in a $D - A$ sample. The equivalence $(\gamma \times I_{Ex_A}^{Em_A}(\lambda))$ is valid if we maintain the equal power for $\lambda_{Ex_D} = 532$ nm.

13. Keeping the coverslip (thin) on the bottom and the glass slide (thick) on the top helps to work in a high-NA objective, which has low working distance.
14. The slit is required for the spatial selection of the object within the field of view (FOV). The slit has to be in the focus of the first image plane. The out-off-focus slit yields an image with a much wider dimension than the expected diffraction limit. Thus, in-focus slit yields higher resolved spatial and thereby spectral (dispersed) image.
15. The zeroth-order image is the intensity image of the object, whereas the first-order image is the dispersed spectra of that emissive object.
16. The narrow slit yields high spectral resolution and prevents the dispersed image from being mixed with the unwanted nearby species.
17. Generally, the phase-separated droplets are not static in the coverslip. If we allow an hour of rest on the microscope stage, then the droplet settled down. It is highly recommended that SR-FRET data remains devoid of motion artifact.
18. The spectral image data collection from $D - A$ sample should be performed first with λ_{Ex_A} followed by λ_{Ex_D}, from the same area. It is imperative to refrain from touching the microscope and producing any mechanical noise to avoid stage drift.
19. The dispersed image of the known laser source through the transmission grating allows us to calibrate the wavelength from pixel to nm. Generally, the power of laser sources, which were used to excite D and A, is increased so that it leaks through the dichroic filters. The remaining lasers easily leak at low power with the existing dichroic set.
20. It is not possible to find the same droplets, which have been imaged in d2. However, the collection of spectra from several droplets with similar size each day represents sufficient knowledge on the nature of interaction among the species.
21. The background subtraction process for a diffraction-limited spot performed in image-based FRET microscopy significantly differs from the SR-FRET microscopy. Generally, the noise has been subtracted from the entire image at once in image-based FRET microscopy.
22. The distance in a pixel has been multiplied by the extracted slope, and the intercept has been added to it. This essentially converts the wavelength in terms of pixel to nm.
23. The emission spectra of droplets containing the only fluorescein-5-maleimide 74C-α-Syn have a very long tail at $\lambda_{Ex_D} = 488nm$. The emission intensity at 595 nm, that is, γ, is found to be ~0.065.

24. It has been found that the rhodamine-C2-maleimide-labeled 74C-α-Syn intensity at 595 nm is ~5.4 times higher when excited at λ_{Ex_A} than when excited at λ_{Ex_D}.
25. In our analysis, the emission spectrum from $D-A$ sample has been normalized with false-positive FRET emission at λ_{Em_A}.
26. It is important to note that in the absence of biomolecular interaction, the intensity enhancement is not expected (i.e., $IEF_{ET} \approx 1$) from the sample. However, when the probe molecules interact, we expect a positive increment of IEF_{ET} (i.e., $IEF_{ET} > 1$) due to energy transfer. Besides, further increase of $\mathrm{IEF_{ET}}$ reflects with higher FRET, that is, more closer association of molecules, either due to the stronger interaction or increase of $D-A$ in the pool of the protein droplets.
27. IEF_{ET} at single droplet levels cannot be exactly equal to the absolute FRET efficiency, which scales with the sixth power of distance (r) for single D and single A dipole-dipole interaction. However, IEF_{ET} is proportional to the FRET efficiency. Note that the excited state of the donor can transfer energy to the nearby acceptor by mechanisms other than FRET. For instance, energy transfer can occur via the electron exchange (Dexter interaction) mechanism when the acceptor is in molecular contact (orbital overlap) with the donor. Besides, in the heterogeneous systems, multiple donors can surround each acceptor as opposed to a single D and single A scenario as in FRET and might experience diverse environments (number and proximity) in different spaces [36].

References

1. Banani SF, Rice AM, Peeples WB et al (2016) Compositional control of phase-separated cellular bodies. Cell 166:651–663
2. Shin Y, Brangwynne CP (2017) Liquid phase condensation in cell physiology and disease. Science 357:eaaf4382
3. Riback JA, Katanski CD, Kear-Scott JL et al (2017) Stress-triggered phase separation is an adaptive, evolutionarily tuned response. Cell 168:1028–1040.e19
4. Banani SF, Lee HO, Hyman AA et al (2017) Biomolecular condensates: Organizers of cellular biochemistry. Nat Rev Mol Cell Biol 18: 285–298
5. Brangwynne CP, Eckmann CR, Courson DS et al (2009) Germline P granules are liquid droplets that localize by controlled dissolution/condensation. Science 324:1729–1732
6. Hyman AA, Weber CA, Jülicher F (2014) Liquid-liquid phase separation in biology. Annu Rev Cell Dev Biol 30:39–58
7. Boeynaems S, Alberti S, Fawzi NL et al (2018) Protein phase separation: a new phase in cell biology. Trends Cell Biol 28:420–435
8. Alberti S (2017) Phase separation in biology. Curr Biol 27:R1097–R1102
9. Holehouse AS, Pappu RV (2018) Functional implications of intracellular phase transitions. Biochemistry 57:2415–2423
10. Feric M, Vaidya N, Harmon TS et al (2016) Coexisting liquid phases underlie nucleolar subcompartments. Cell 165:1686–1697
11. Kaiser TE, Intine RV, Dundr M (2008) De novo formation of a subnuclear body. Science 322:1713–1717
12. Lin Y, Protter DSW, Rosen MK et al (2015) Formation and maturation of phase-separated

liquid droplets by RNA-binding proteins. Mol Cell 60:208–219
13. Brangwynne CP, Tompa P, Pappu RV (2015) Polymer physics of intracellular phase transitions. Nat Phys 11:899–904
14. Wei MT, Elbaum-Garfinkle S, Holehouse AS et al (2017) Phase behaviour of disordered proteins underlying low density and high permeability of liquid organelles. Nat Chem 9: 1118–1125
15. Molliex A, Temirov J, Lee J et al (2015) Phase separation by low complexity domains promotes stress granule assembly and drives pathological fibrillization. Cell 163:123–133
16. Nott TJ, Petsalaki E, Farber P et al (2015) Phase transition of a disordered nuage protein generates environmentally responsive membraneless organelles. Mol Cell 57:936–947
17. Zhang H, Elbaum-Garfinkle S, Langdon EM et al (2015) RNA controls polyQ protein phase transitions. Mol Cell 60:220–230
18. Vecchi G, Sormanni P, Mannini B et al (2020) Proteome-wide observation of the phenomenon of life on the edge of solubility. Proc Natl Acad Sci USA 117:1015–1020
19. Boke E, Ruer M, Wühr M et al (2016) Amyloid-like self-assembly of a cellular compartment. Cell 166:637–650
20. Murakami T, Qamar S, Lin JQ et al (2015) ALS/FTD mutation-induced phase transition of FUS liquid droplets and reversible hydrogels into irreversible hydrogels impairs RNP granule function. Neuron 88:678–690
21. Patel A, Lee HO, Jawerth L et al (2015) A liquid-to-solid phase transition of the ALS protein FUS accelerated by disease mutation. Cell 162:1066–1077
22. Wegmann S, Eftekharzadeh B, Tepper K et al (2018) Tau protein liquid–liquid phase separation can initiate tau aggregation. EMBO J 37: e98049
23. Ambadipudi S, Biernat J, Riedel D et al (2017) Liquid-liquid phase separation of the microtubule-binding repeats of the Alzheimer-related protein Tau. Nat Commun 8:275
24. Conicella AE, Zerze GH, Mittal J et al (2016) ALS mutations disrupt phase separation mediated by α-helical structure in the TDp-43 low-complexity c-terminal domain. Structure 24:1537–1549
25. Ray S, Singh N, Kumar R et al (2020) α-Synuclein aggregation nucleates through liquid–liquid phase separation. Nat Chem 12: 705–716
26. Goldman RD, Spector DL, Masters BR (2006) Live cell imaging, a laboratory manual. J Biomed Opt 11:019901
27. Bolte S, Cordelières FP (2006) A guided tour into subcellular colocalization analysis in light microscopy. J Microsc 224:213–232
28. Hu K, Johnson J, Florens L, Fraunholz M et al (2006) Cytoskeletal components of an invasion machine – the apical complex of Toxoplasma gondii. PLoS Pathog 2:0121–0138
29. Kumar P, Lyle KS, Gierke S et al (2009) GSK33 phosphorylation modulates CLASP-microtubule association and lamella microtubule attachment. J Cell Biol 184:895–908
30. Waters JC (2009) Accuracy and precision in quantitative fluorescence microscopy. J Cell Biol 185:1135–1148
31. Gordon GW, Berry G, Liang XH et al (1998) Quantitative fluorescence resonance energy transfer measurements using fluorescence microscopy. Biophys J 74:2702–2713
32. Zeug A, Woehler A, Neher E, Ponimaskin EG (2012) Quantitative intensity-based FRET approaches – a comparative snapshot. Biophys J 103:1821–1827
33. Pentcheva T, Edidin M (2001) Clustering of peptide-loaded MHC class I molecules for endoplasmic reticulum export imaged by fluorescence resonance energy transfer. J Immunol 166:6625–6632
34. Andrews DL (1989) A unified theory of radiative and radiationless molecular energy transfer. Chem Phys 135:195–201
35. Sekar RB, Periasamy A (2003) Fluorescence resonance energy transfer (FRET) microscopy imaging of live cell protein localizations. J Cell Biol 160:629–633
36. Lakowicz JR (2006) Principles of fluorescence spectroscopy. Springer, US, Boston, MA
37. Kenworthy AK (2001) Imaging protein-protein interactions using fluorescence resonance energy transfer microscopy. Methods 24:289–296
38. Periasamy A (2001) Fluorescence resonance energy transfer microscopy: a mini review. J Biomed Opt 6:287
39. Lemke EA, Deniz AA (2011) Förster resonance energy transfer. In: Comprehensive nanoscience and technology. Elsevier, pp 127–151
40. Berney C, Danuser G (2003) FRET or no FRET: a quantitative comparison. Biophys J 84:3992–4010
41. Kapanidis AN, Laurence TA, Nam KL et al (2005) Alternating-laser excitation of single molecules. Acc Chem Res 38:523–533

42. Das S, Sharma DK, Chakrabarty S et al (2015) Bioactive polymersomes self-assembled from amphiphilic PPO-glyco polypeptides: Synthesis, characterization, and dual-dye encapsulation. Langmuir 31:3402–3412
43. Sarkar A, Behera T, Sasmal R et al (2020) Cooperative supramolecular block copolymerization for the synthesis of functional axial organic heterostructures. J Am Chem Soc 142:11528–11539
44. Bates M, Jones SA, Zhuang X (2013) Stochastic optical reconstruction microscopy (STORM): a method for superresolution fluorescence imaging. Cold Spring Harb Protoc 8: 498–520
45. Möckl L, Lamb DC, Bräuchle C (2014) Superresolved fluorescence microscopy: Nobel prize in chemistry 2014 for Eric Betzig, Stefan Hell, and William E. Moerner. Angew Chemie Int Ed Engl 53:13972–13977